

# Fast Learning-based Registration of Sparse 3D Clinical Images

**Kathleen M. Lewis**

*Computer Science and Artificial Intelligence Laboratory (CSAIL), MIT*

**Natalia S. Rost**

*Massachusetts General Hospital, Harvard Medical School*

**John Guttag**

*Computer Science and Artificial Intelligence Laboratory (CSAIL), MIT*

**Adrian V. Dalca**

*Computer Science and Artificial Intelligence Laboratory (CSAIL), MIT*

*Massachusetts General Hospital, Harvard Medical School*

## Abstract

We introduce SparseVM, a method to register clinical 3D scans faster and more accurately than previously possible. Deformable alignment, or registration, of clinical scans is a fundamental task for many medical image applications such as longitudinal population studies. Most registration algorithms are designed for high-resolution research-quality scans and under-perform when applied to clinical data. Clinical scans present unique challenges because, in contrast to research-quality scans, clinical scans are often sparse, missing up to 85% of the slices available in research scans. We build on a state-of-the-art learning-based registration method to improve the accuracy of sparse clinical image registration and demonstrate our method on a clinically-acquired MRI dataset of stroke patients. SparseVM registers 3D scans in under a second on a GPU, which is over  $1000\times$  faster than the most accurate clinical registration methods, without compromising accuracy. Because of this, SparseVM enables clinical analyses that were not previously possible. The code is publicly available at [voxelmorph.mit.edu](http://voxelmorph.mit.edu).

## 1. Introduction

Deformable medical image registration establishes a dense, non-linear correspondence between a pair of medical scans and is a fundamental step in medical image analyses such as longitudinal population studies. Most existing registration methods focus on high-resolution research-quality scans. In contrast, clinical settings often require limited scanning time because of patient safety and financial constraints. For 3D imaging modalities such as MRI, this often means a few 2D slices are acquired instead of a dense 3D volume, leading to spatially sparse scans. Each 2D slice can be high resolution, but the 3D volume can be missing up to 85% of the slices that are typically available in a research-quality scan. The wide spacing between slices causes drastic discontinuities in anatomy between neighboring slices (Fig. 1). Furthermore, the anatomy captured by the slices is not consistent across different scans; depending on the orientation of the patient with respect to the scanner, different anatomy may be present in the acquired slices.

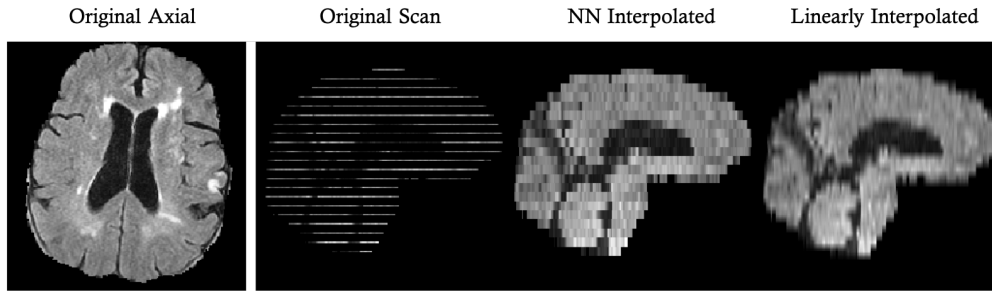


Figure 1: Example stroke subject scan with corresponding interpolated images. The subject scan has approximately 15% of the slices normally available in a full resolution research quality scan. Shown from left to right are an axial slice from the original scan, the original subject slices seen from a sagittal view, nearest neighbor (NN) interpolated image, and linearly interpolated image.

Most classical registration methods are designed for full-resolution scans rather than sparse clinical scans. Successful methods include elastic-type models (Bajcsy and Kovacic, 1989; Shen and Davatzikos, 2002; Davatzikos, 1997), statistical parametric mapping (Ashburner and Friston, 2000), free-form deformations with b-splines (Rueckert et al., 1999), discrete methods (Glocker et al., 2008), and Demons (Thirion, 1998; Pennec et al., 1999). Diffeomorphic transforms explicitly enforce topology constraints, and have been thoroughly studied (Beg et al., 2005; Miller et al., 2005; Ashburner, 2007; Vercauteren et al., 2009; Avants et al., 2008a). All of these non-learning based methods require solving a high dimensional optimization on each new pair of scans and therefore have slow runtimes. Moreover, applying these methods to clinical scans is problematic because they were developed to work on high resolution scans and require spatial continuity for smooth image gradients, which are not available in clinical scans.

A recent patch-based registration method (Dalca et al., 2016) builds on discrete registration methods by explicitly accounting for sparsity in clinical data and avoiding dependence on spatial gradients. This method accurately registers clinical scans, but takes on the order of two hours to register a single pair of scans.

In contrast to classical registration methods, recent learning-based methods are significantly faster. These methods are designed for high-resolution scans. Learning-based registration methods use neural networks to learn a function that takes in two scans as input and outputs a deformation field. Many are supervised, requiring ground truth warp fields (Roh et al., 2017; Sokooti et al., 2017; Yang et al., 2017; Cao et al., 2017). Recent unsupervised methods (Balakrishnan et al., 2018a,b; Dalca et al., 2018a; de Vos et al., 2017; Li and Fan, 2017) have been shown to work well on research quality, high resolution scans.

**Technical Significance** In this work, we build upon an open-source unsupervised learning-based method, VoxelMorph, to achieve very fast and accurate registration of both sparse clinical scans and research scans. We design a new loss function, sparse local cross correlation (SLCC), which weights voxel contributions in proportion to confidence in the voxel

observations. We demonstrate that our method is 1) more than  $1000\times$  faster than the best classical methods without losing accuracy and 2) more accurate than current learning-based methods.

**Clinical Relevance** We demonstrate our method on a clinical study of stroke patients containing T2-FLAIR MR brain scans (Rost et al., 2010). Currently the registration methods designed for clinical data take on the order of two hours to register a pair of scans, while the fast learning-based methods are not accurate enough on clinical scans. Therefore, with existing methods, researchers and clinicians have to make a trade-off between speed and accuracy when registering clinical scans. Our method takes less than a second on a GPU to register a pair of scans, while achieving equivalent or higher accuracy than all state-of-the-art methods. This facilitates population analyses that were previously infeasible and promises to extend to uses in the clinic.

## 2. Methods

Let  $f, m$  be two volumes defined over a 3D spatial domain  $\Omega \subset \mathbb{R}^3$ . We assume  $f$  and  $m$  contain grayscale data and are affinely aligned as a preprocessing step, so that the scan pairs only exhibit non-rigid misalignments. We use one of the several available affine alignment packages, which roughly work for both clinical and research images.

We build on the learning-based method VoxelMorph (Balakrishnan et al., 2018a,b; Dalca et al., 2018a) to accurately register clinical scans. VoxelMorph is an unsupervised method that uses a convolutional neural network to learn a function,  $g_\theta(f, m) = \phi$ , to compute a deformation field  $\phi$  for a pair of given scans  $\{f, m\}$ . At test time, VoxelMorph evaluates this function on two input scans and outputs the deformation field  $\phi$ , as well as the registered image,  $w_m = m \circ \phi$  ( $m$  warped by  $\phi$ ). VoxelMorph was developed for high resolution isotropic scans. We design a method based on VoxelMorph to address the problem of sparsity in clinical scans.

### 2.1. Loss Functions

We first describe the loss functions used in VoxelMorph as well as other registration methods, and in the next section we propose loss functions designed for clinical data.

Most medical image registration methods optimize a loss function of the form:

$$L(f, m, \phi) = L_{sim}(f, m \circ \phi) + \lambda L_{smooth}(\phi), \quad (1)$$

where  $\lambda$  is a regularization hyperparameter. This loss function balances an image matching term  $L_{sim}$  with a regularization or spatial smoothness term  $L_{smooth}$ . The first term measures the similarity in appearance between the fixed image  $f$  and the warped image  $w_m$ . The second term encourages the displacement field  $\phi$  to be smooth and anatomically realistic. This loss is used in learning-based methods to learn the global network parameter  $\theta$ , where  $\phi = g_\theta(\cdot, \cdot)$ .

Intensity mean-squared error (MSE) and cross correlation (CC) are the most commonly used similarity measures. MSE compares intensities at each voxel (2):

$$MSE(f, w_m) = \frac{1}{|\Omega|} \sum_{p \in \Omega} [f(p) - w_m(p)]^2, \quad (2)$$

where the notation  $f(p)$  indicates the value of image  $f$  at voxel location  $p$ .

Local cross correlation has been shown to be more invariant than MSE to differences in intensity distributions across scans (Avants et al., 2008b). For scans  $f$  and  $m$ , let  $\mu_f(p)$  and  $\mu_{w_m}(p)$  be the local neighborhood intensity mean around voxel  $p$ :  $\mu_f(p) = \frac{1}{n^3} \sum_{p_i} f(p_i)$ , where  $n^3$  is the neighborhood size and  $p_i$  iterates over the  $n^3$  volume of voxels surrounding voxel  $p$ . The local cross correlation is then:

$$LCC(f, w_m) = \sum_{p \in \Omega} \frac{[\sum_{p_i} (f(p_i) - \mu_f(p))(w_m(p_i) - \mu_{w_m}(p))]^2}{[\sum_{p_i} (f(p_i) - \mu_f(p))^2][\sum_{p_i} (w_m(p_i) - \mu_{w_m}(p))^2]}. \quad (3)$$

The  $L_{smooth}$  loss often penalizes the local spatial gradients of  $u$ ,  $\nabla u$ , where  $u$  is the vector displacement such that  $\phi = Id + u$  and  $Id$  is the identity transform:

$$L_{smooth}(\phi) = \sum_{p \in \Omega} \|\nabla u(p)\|^2. \quad (4)$$

## 2.2. Sparse Method

We propose two new image similarity losses that generalize Eq. (2) and Eq. (3) and lead to accurate registration on both clinical and high resolution scans. We upsample each clinical image to isotropic spatial resolution (equal resolution in all planes) by linearly interpolating between the acquired slices (Fig. 1, right).

Our new loss functions use masks,  $m_f$  and  $m_m$ , corresponding to the fixed image  $f$  and the moving image  $m$ , respectively. In its simplest form, each voxel in a mask has a value of 0 (interpolated voxel) or 1 (acquired voxel). We let  $m_c = m_f * m_m$  be a combined mask that indicates voxels that are observed in both scans, where  $*$  denotes element-wise multiplication.

We define sparse mean squared error (SMSE) which generalizes Eq. (2) by calculating the loss over only observed voxels:

$$SMSE(f, m_c, w_m) = \frac{1}{\sum m_c(p)} \sum_{p \in \Omega} [f(p) - w_m(p)]^2 m_c(p). \quad (5)$$

The implementation of sparse local cross correlation (SLCC) is less straightforward since it requires careful treatment of correlating the sparsely observed voxels. For each image, we compute the local mean of each neighborhood over only the observed voxels:

$$\mu_f(p) = \frac{1}{\sum_{p_i \in n^3} m_f(p_i)} \sum_{p_i \in n^3} f(p_i) m_f(p_i). \quad (6)$$

We define  $\hat{f}(p_i, p)$  at voxel  $p_i$  belonging to a neighborhood centered at  $p$  as the image with the local mean subtract out:

$$\hat{f}(p_i, p) = f(p_i) - \mu_f(p). \quad (7)$$

Finally we define the sparse local cross correlation as:

$$SLCC(f, m_c, w_m) = \sum_{p \in \Omega} \frac{[\sum_{p_i \in n^3} m_c(p_i) \hat{f}_i(p_i, p) \hat{w}_{mi}(p_i, p)]^2}{[\sum_{p_i \in n^3} m_c(p_i) \hat{f}_i(p_i, p)^2][\sum_{p_i \in n^3} m_c(p_i) \hat{w}_{mi}(p_i, p)^2]}, \quad (8)$$

where, as before,  $i \in n^3$  indicate a voxel  $i$  in the neighborhood  $n^3$  centered around  $p$ .

SLCC computes the local correlation in each neighborhood between voxels that are observed in both scans. Since SLCC does not use values over unobserved (interpolated) voxels, the neighborhoods are sparse. As in regular local cross correlation, the neighborhood size  $n^3$  is a hyperparameter. In SLCC, special care must be taken to ensure the neighborhoods are large enough to contain enough non-zero voxels, but small enough to capture specific regions of the scans.

The smoothness constraint on the deformation field remains the same (Eq.4) regardless of whether the data is sparse or not.

### 3. Experiments

In our experiments, we focus on atlas-based registration and use a full-resolution atlas, or reference image, computed with the help of an external dataset (Sridharan et al., 2013). In atlas-based registration, we register the atlas to each subject scan. This is often used in population studies, where inter-subject registration is a core problem. We demonstrate our method on a clinically acquired MRI dataset for stroke patients (Rost et al., 2010).

#### 3.1. Datasets

The dataset contains T2-FLAIR MR scans acquired within 48 hours of stroke onset in a patient cohort. The in-plane resolution is 0.85 mm and the spacing between slices ranges between 5-7mm. The dataset contains manual segmentations of the ventricles for 104 of the subjects. The 237 subjects without manual segmentations were used for training, while the 104 subjects with manual segmentations were split into validation (29 subjects) and test (75 subjects) sets.

During pre-processing the scans were affinely-aligned to the atlas and skull-stripped using an existing toolbox (Sridharan et al., 2013). The atlas  $m$  in our atlas-based registration experiments is isotropic, and therefore  $m_m$  consists of value 1 at each voxel. In contrast,  $f$  has approximately 15% of the number of acquired slices of an isotropic research scan, and we linearly interpolate the remaining slices to achieve the same resolution as the atlas. The scans were then padded to be 160x192x160 voxels. The subject mask  $m_f(p)$  is one for voxels  $p$  in the acquired slices and zero for voxels  $p$  in the interpolated slices. To perform affine alignment, both  $f$  and  $m_f$  are resampled, and voxels are therefore linearly interpolated. The final mask values in  $m_f$  are continuous in the range  $[0, 1]$ . We interpret these values as weightings of confidence where voxels with low values do not contain information from the acquired slices.

#### 3.2. Baseline Methods

We compare our method to VoxelMorph (Balakrishnan et al., 2018a) as well as the state-of-the-art clinical image registration method Patch Based Registration (PBR) (Dalca et al., 2016). PBR is a patch-based iterative discrete registration method that explicitly accounts for sparsity in clinical data. We also compare against the widely used Advanced Normalization Tools software package (ANTs) (Avants et al., 2011), which is used as a baseline in the original VoxelMorph and PBR papers. We use the cross correlation loss for ANTs.

Method	Average (SD)	Median (MAD)	GPU sec	CPU sec
ANTs (optimized)	0.696 (0.070)	0.720 (0.050)	-	9059 (2023)
PBR (best)	0.732 (0.071)	0.749 (0.052)	-	9269 (5134)
VoxelMorph CC15	0.723 (0.077)	0.748 (0.060)	0.283 (0.028)	37.1 (2.78)
SparseVM SMSE	0.719 (0.075)	0.740 (0.058)	0.303 (0.047)	41 (0.584)
SparseVM SLCC	<b>0.743 (0.076)</b>	<b>0.768 (0.060)</b>	<b>0.241 (0.030)</b>	<b>32.7 (0.452)</b>

Table 1: Dice scores and test runtimes for ANTs, PBR, VoxelMorph, and SparseVM on the stroke dataset. The average Dice score and median Dice score are computed for all test subjects on the left and right lateral ventricle labels. The standard deviation and median absolute deviation are shown in parentheses. The runtimes are calculated after pre-processing. SparseVM using SLCC is both more accurate and faster than the baselines.

For all baseline methods, we used the optimal parameters given in the original publications, except for the cross correlation neighborhood size. In the original VoxelMorph paper, a cross correlation neighborhood size of  $9^3$  is used. However, from our experiments we found a larger neighborhood size of  $15^3$  leads to better performance. This is likely due to the sparsity of the neighborhoods in clinical data as explained previously in Section 2.2.

### 3.3. Evaluation Metric

We evaluate registration performance quantitatively using the Dice metric (Dice, 1945) and qualitatively using visual evaluation. Dice measures the volume overlap of anatomical segmentations and ranges between 0 and 1, with 0 representing no overlap and 1 representing perfect overlap. We use the output deformation field to warp the ventricle segmentations of the atlas to the subject and compare to the manual subject segmentations. We then compute Dice in the subject space in acquired slices (e.g. Figure 4).

### 3.4. Implementation

We implement SparseVM using Keras (Chollet et al., 2015) with a TensorFlow backend (Abadi et al., 2016). We use the ADAM optimizer (Kingma and Ba, 2014) with an epsilon value of  $5e-5$  and a learning rate of  $5e-4$ . We use the architecture proposed in the original VoxelMorph paper (Balakrishnan et al., 2018a), which is publicly available online. For SLCC, we use sparse convolutional layers (Dalca et al., 2018b).

For the smoothness regularization hyperparameter  $\lambda$ , we use the value used in the original VoxelMorph papers to guide our parameter search. We then use the validation set to choose the best parameter value. We implement SLCC with a neighborhood size  $n=15$ , which we found to perform well given the sparsity in our data.

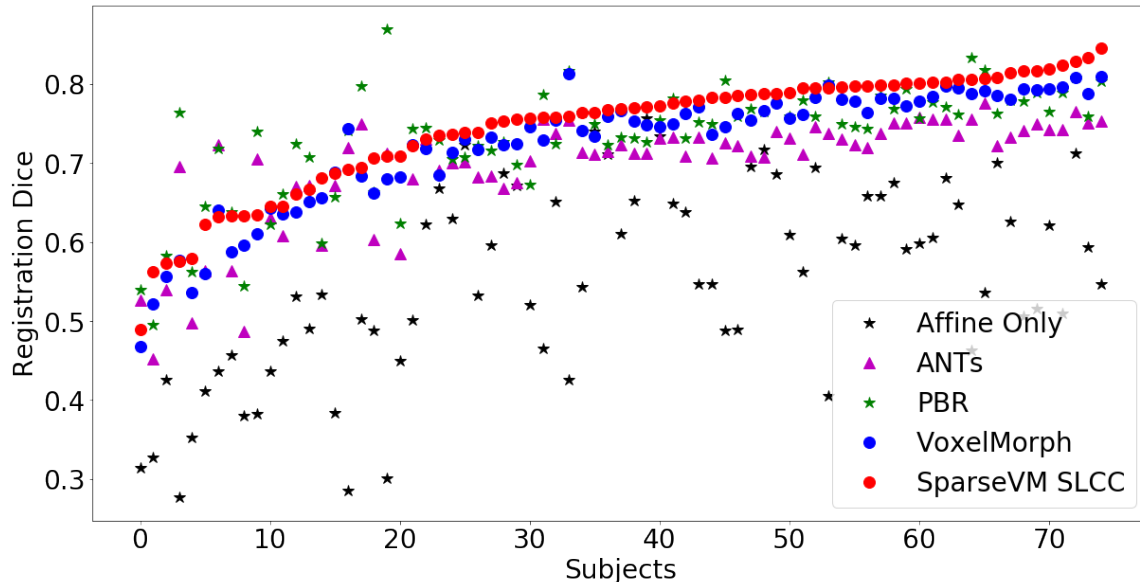


Figure 2: Dice score for each subject sorted by SparseVM performance. SparseVM using SLCC is better than ANTs on 86.7% of test subjects, better than PBR on 69.3% of test subjects, and better than VoxelMorph on 90.7% of test subjects.

## 4. Results

### 4.1. Quantitative Comparison with Baselines

Table 1 summarizes the average and median Dice scores for all test subjects on the ventricles, and the average test runtimes of each method. SparseVM has 1) the highest average highest median Dice scores and 2) the fastest runtime.

Both ANTs and PBR take on the order of two hours on a CPU, while VoxelMorph and SparseVM take less than a minute on a single-threaded CPU and less than a second on a GPU. SparseVM’s improvement in runtime is statistically significant over the most accurate baseline, PBR, with a p-value of  $3.76e-17$  using a paired t-test. There are no GPU implementations of ANTs or PBR.

Since the registration results for different subjects exhibit high variance, as shown by the standard deviations, we also show the Dice for each subject in Figure 2. SparseVM using SLCC outperforms ANTs on 86.7% of test subjects, PBR on 69.3% of test subjects, and VoxelMorph on 90.7% of test subjects. We perform additional analyses on learning-based registration methods, which are the only methods feasible for large-scale analyses involving hundreds or thousands of scans. We plot the subject-wise difference in Dice accuracy between SparseVM and VoxelMorph in Figure 3. The pairwise improvement in accuracy of SparseVM is statistically significant with a p-value of  $1.60e-14$  using a paired t-test. SparseVM yields an average improvement of two Dice points over VoxelMorph.



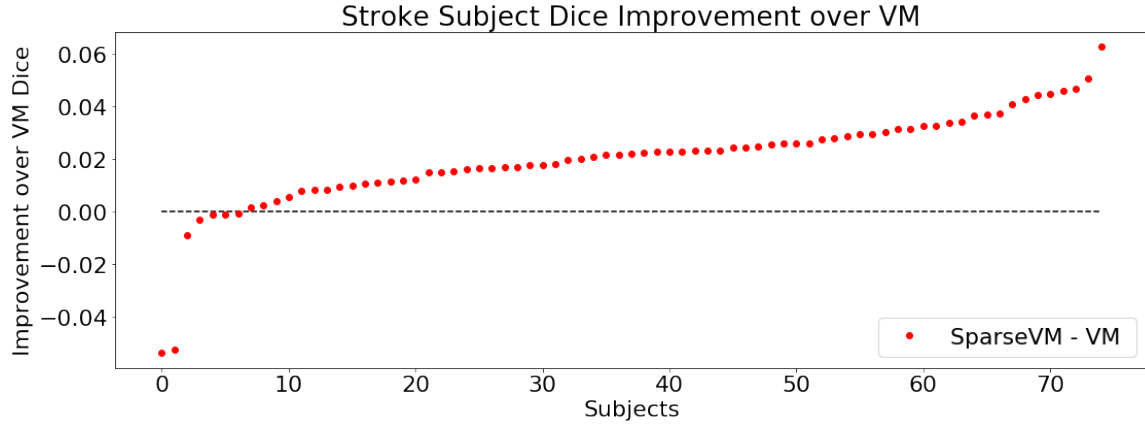


Figure 3: Dice improvement of SparseVM results over VoxelMorph results per subject sorted in increasing order of improvement. SparseVM has higher Dice scores on 90.7% of the subjects and is on average 2 Dice better than VoxelMorph. Upon visual inspection, we find that the first two subjects were aggressively skull-stripped such that part of the brain was removed.

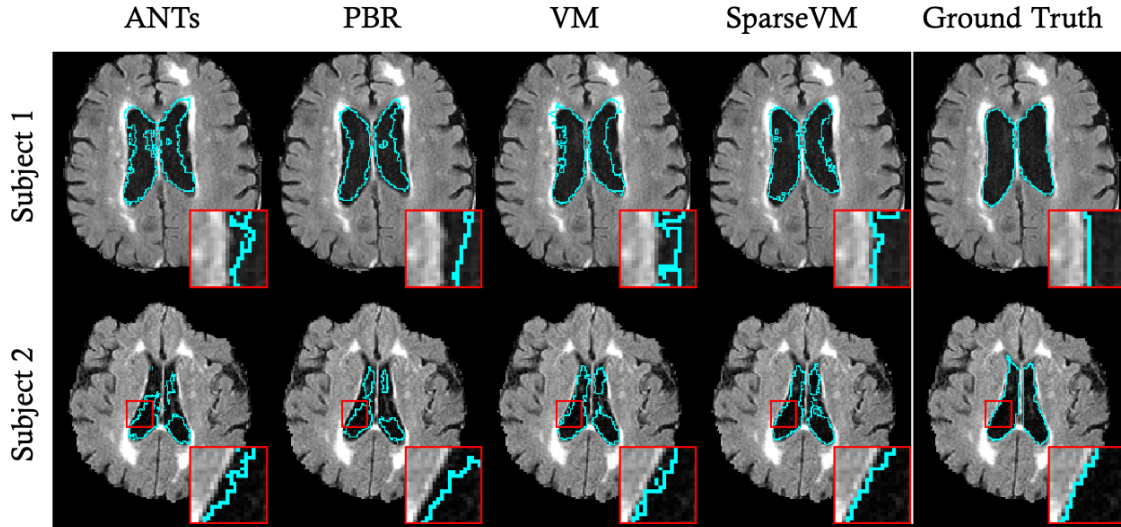


Figure 4: Example results. Warped atlas segmentations overlaid on the subject scan for subjects with different sized ventricles.

## 4.2. Qualitative Analysis

Figure 4 shows registration results for several test subjects, illustrating the intensity heterogeneity present in these patients. This visualization enables a closer examination of the results. By evaluating specific regions of the brain, we observe that SparseVM provides reg-



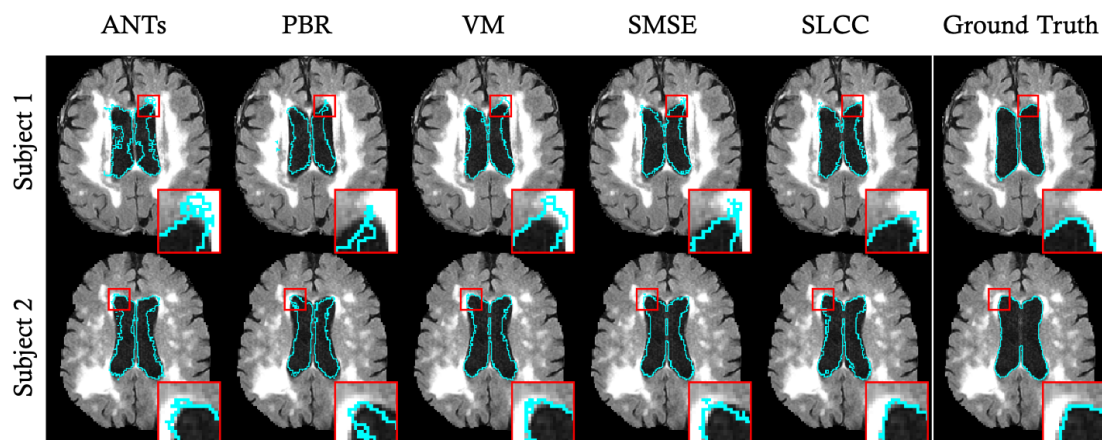


Figure 5: Example results. Warped atlas segmentations overlaid on the subject scan for subjects with high WMH burden.

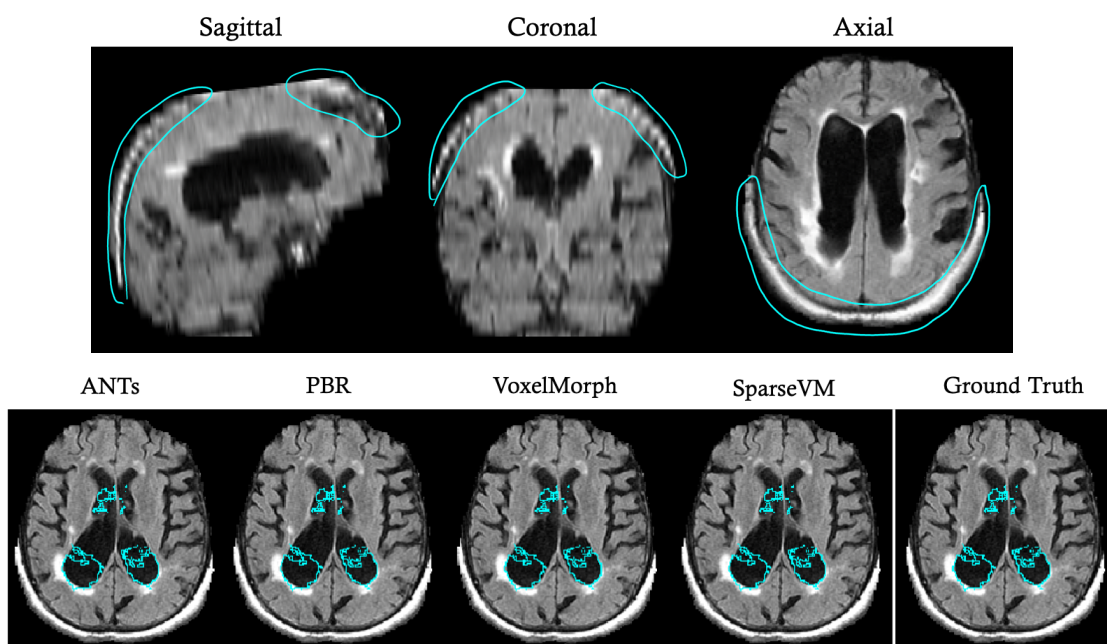


Figure 6: Example test subject that was not properly skull stripped during pre-processing. The top row highlights examples of areas where skull is present in the scan. The bottom row shows the warped atlas segmentations for each method. The PBR segmentations cover most of the ventricles, while the other methods only segment part of the ventricles.

istration that enables, for example, the ventricle segmentations to better snap to the actual anatomical boundaries. Consistent with our quantitative results, the close-up regions show that warped atlas segmentations using PBR, VM, and SparseVM outperform the popular toolbox ANTS, with SparseVM (SLCC) performing optimally among these methods.

We also characterize subjects for which SparseVM using SLCC performs worse than a baseline. By visualizing such subjects in a manner similar to Figure 4, we find that SparseVM using SLCC tends to perform worse on subjects for which skull-stripping or affinely alignment fails during pre-processing. Figure 6 shows an example of a test subject that has not been properly skull stripped. Affine alignment and skull-stripping algorithms for clinical data are current areas of research.

The original study that resulted in the stroke dataset investigated white matter hyperintensity (WMH) burden in stroke patients (Rost et al., 2010). WMH is an important predictor of future cardiovascular health and is visible in the T2 FLAIR scans. However, differences in intensities caused by WMH add to the difficulty of clinical registration. Therefore we also visually analyze the registration performance of SparseVM near regions of significant WMH burden. We find that SparseVM using SLCC leads to better performance than SparseVM using SMSE for subjects with high WMH, likely because of the robustness of local cross correlation to intensity heterogeneity. Figure 5 shows example subjects with high WMH burden. In most areas of the brain, SparseVM performs comparably or much better than the other methods.

## 5. Conclusion

We introduce SparseVM, a fast unsupervised method that can accurately register sparse, low-resolution clinical scans. SparseVM significantly and meaningfully improves performance accuracy over VoxelMorph while maintaining comparable speed. SparseVM is over  $1000\times$  faster than other methods that achieve state-of-the-art accuracy for clinical image registration, while achieving comparable or better Dice scores. Since SparseVM can accurately register pairs of clinical scans in under a second on the GPU, it enables clinical image analyses that were not previously possible. For example, many medical population analyses involving tens of thousands of subjects were previously infeasible or would take months of computation. With our method, these analyses are now possible in minutes or hours. We are actively working on porting SparseVM to the clinical setting to be used in large clinical studies.

## Acknowledgments

This project was funded in part by the Wistron Corporation.

## References

- M. Abadi, P. Barham, J. Chen, Z. Chen, A. Davis, J. Dean, M. Devin, S. Ghemawat, G. Irving, M. Isard, et al. Tensorflow: Large-scale machine learning on heterogeneous distributed systems. *arXiv:1603.04467*, 2016.

- J. Ashburner. A fast diffeomorphic image registration algorithm. *Neuroimage*, 38(1):95–113, 2007.
- J. Ashburner and K. Friston. Voxel-based morphometry-the methods. *Neuroimage*, 11: 805–821, 2000.
- B. B. Avants, C. L. Epstein, M. Grossman, , and J. C. Gee. Symmetric diffeomorphic image registration with cross-correlation: evaluating automated labeling of elderly and neurodegenerative brain. *Medical image analysis*, 12(1):26–41, 2008a.
- B. B. Avants, C. L. Epstein, M. Grossman, and J. C. Gee. Symmetric diffeomorphic image registration with cross-correlation: evaluating automated labeling of elderly and neurodegenerative brain. *Medical image analysis*, 12(1):26–41, 2008b.
- B.B Avants, N. J. Tustison, G. Song, P. A. Cook, A. Klein, and J. C. Gee. A reproducible evaluation of ants similarity metric performance in brain image registration. *Neuroimage*, 54(3):2033–2044, 2011.
- R. Bajcsy and S. Kovacic. Multiresolution elastic matching. *Computer Vision, Graphics, and Image Processing*, 46:1–21, 1989.
- G. Balakrishnan, A. Zhao, M. R. Sabuncu, J. Guttag, and A. V. Dalca. An unsupervised learning model for deformable medical image registration. Proceedings of the IEEE Conference on Computer Vision and Pattern Recognition, 2018a.
- G. Balakrishnan, A. Zhao, M. R. Sabuncu, J. Guttag, and A. V. Dalca. Voxel-morph: A learning framework for deformable medical image registration. *arXiv preprint arXiv:1809.05231*, 2018b.
- M. F. Beg, M. I. Miller, A. Trounev, and L. Younes. Computing large deformation metric mappings via geodesic flows of diffeomorphisms. *Int. J. Comput. Vision*, 61:139–157, 2005.
- X. Cao, J. Yang, J. Zhang, D. Nie, M. Kim, Q. Wang, and D. Shen. Deformable image registration based on similarity-steered cnn regression. pages 300–308. International Conference on Medical Image Computing and Computer-Assisted Intervention, Springer, 2017.
- F. Chollet et al. Keras. <https://github.com/fchollet/keras>, 2015.
- A. V. Dalca, A. Bobu, N. S. Rost, and P. Golland. Patch-based discrete registration of clinical brain images. pages 60–67. International Workshop on Patch-based Techniques in Medical Imaging, Springer, 2016.
- A. V. Dalca, G. Balakrishnan, J. Guttag, and M. R. Sabuncu. Unsupervised learning for fast probabilistic diffeomorphic registration. volume 11070, pages 729–738. MICCAI: Int. Conf. on Medical Image Computing and Computer Assisted Intervention., LNCS, 2018a.
- A. V. Dalca, J. Guttag, and M. R. Sabuncu. Anatomical priors in convolutional networks for unsupervised biomedical segmentation. pages 9290–9299. Proceedings of the IEEE Conference on Computer Vision and Pattern Recognition, 2018b.

- C. Davatzikos. Spatial transformation and registration of brain images using elastically deformable models. *Computer Vision and Image Understanding*, 66(2):207–222, 1997.
- B. de Vos, F. F. Berendsen, Viergever M. A., M. Staring, and I. Išgum. End-to-end unsupervised deformable image registration with a convolutional neural network. *Deep Learning in Medical Image Analysis and Multimodal Learning for Clinical Decision Support*, pages 204–212, 2017.
- L.R. Dice. Measures of the amount of ecologic association between species. *Ecology*, 26(3):297–302, 1945.
- B. Glocker, N. Komodakis, G. Tziritas, N. Navab, and N. Paragios. Dense image registration through mrfs and efficient linear programming. *Medical image analysis*, 12(6):731–741, 2008.
- D. P. Kingma and J. Ba. Adam: A method for stochastic optimization. *arXiv preprint arXiv:1412.6980*, 2014.
- H. Li and Y. Fan. Non-rigid image registration using fully convolutional networks with deep self-supervision. *arXiv*, 2017.
- M. I. Miller, M. F. Beg, C. Ceritoglu, and C. Stark. Increasing the power of functional maps of the medial temporal lobe by using large deformation diffeomorphic metric mapping. *Proceedings of the National Academy of Sciences*, 102(27):9685–9690, 2005.
- X. Pennec, P. Cachier, and N. Ayache. Understanding the “demon’s algorithm”: 3d non-rigid registration by gradient descent. pages 597–605, 1999.
- M.-M. Roh, M. Datar, T. Heimann, M. Sermesant, and X. Pennec. Svf-net: Learning deformable image registration using shape matching. pages 266–274. International Conference on Medical Image Computing and Computer-Assisted Intervention (MICCAI), Springer, 2017.
- NS Rost, K. Fitzpatrick, A. Biffi, A. Kanakis, W. Devan, C. D. Anderson, L. Cortellini, K. L. Furie, and J. Rosand. White matter hyperintensity burden and susceptibility to cerebral ischemia. *Stroke*, 42(12):2807–2811, 2010.
- D. Rueckert, L. I. Sonoda, C. Hayes, D. L. Hill, M. O. Leach, and D. J. Hawkes. Non-rigid registration using free-form deformation: Application to breast mr images. *IEEE Transactions on Medical Imaging*, 18(8):712–721, 1999.
- D. Shen and C. Davatzikos. Hammer: Hierarchical attribute matching mechanism for elastic registration. *IEEE Transactions on Medical Imaging*, 21(11):1421–1439, 2002.
- H. Sokooti, B. de Vos, F. Berendsen, B. P. Levieveltdt, I. Išgum, and M. Staring. Nonrigid image registration using multi-scale 3d convolutional neural networks. pages 232–239. International Conference on Medical Image Computing and Computer-Assisted Intervention (MICCAI), Springer, 2017.

- R. Sridharan, A. V. Dalca, K. M. Fitzpatrick, L. Cloonan, A. Kanakis, O. Wu, K. L. Furie, J. Rosand, N. S. Rost, , and P. Golland. Quantification and analysis of large multimodal clinical image studies: Application to stroke. pages 18–30. International Workshop on Multimodal Brain Image Analysis, Springer, 2013.
- J. Thirion. Image matching as a diffusion process: an analogy with maxwell’s demons. *Medical Image Analysis*, 2(3):243–260, 1998.
- T. Vercauteren, X. Pennec, A. Perchant, and N. Ayache. Diffeomorphic demons: Efficient non-parametric image registration. *Neuroimage*, 45(1):S61–S72, 2009.
- X. Yang, R. Kwitt, M. Styner, and M. Niethammer. Quicksilver: Fast predictive image registration- a deep learning approach. *NeuroImage*, 158:378–396, 2017.